Hypoxia triggers collective aerotactic migration in *Dictyostelium discoideum*

O. Cochet-Escartin[1]*, M. Demircigil[2], S. Hirose[3,4], B. Allais[1], P. Gonzalo[5,6], I. Mikaelian[5], K. Funamoto[3,4,7], C. Anjard[1], V. Calvez[2]*, J.-P. Rieu[1]*

Affiliations:

1-Institut Lumière Matière, UMR5306, Université Lyon 1-CNRS, Université de Lyon, 69622 Villeurbanne, France.

2- Institut Camille Jordan, UMR5208, Université Lyon 1-CNRS, Université de Lyon, 69622 Villeurbanne, France.

3- Graduate School of Biomedical Engineering, Tohoku University, 6-6-12 Aramaki-aza Aoba, Aoba-ku, Sendai, Miyagi 980-8579, Japan.

4- Institute of Fluid Science, Tohoku University, 2-1-1 Katahira, Aoba-ku, Sendai, Miyagi 980-8577, Japan.

5- Centre Léon Bérard, Centre de recherche en cancérologie de Lyon, INSERM 1052, CNRS 5286, Université Lyon 1, Université de Lyon, 69373, Lyon, France.

6- Laboratoire de Biochimie et Pharmacologie, Faculté de médecine de Saint-Etienne, CHU de Saint-Etienne, 42000, Saint-Etienne, France.

7- Graduate School of Engineering, Tohoku University, 6-6 Aramaki-aza Aoba, Aoba-ku, Sendai, Miyagi 980-8579, Japan.

*Corresponding authors:

Olivier Cochet-Escartin, olivier.cochet-escartin@univ-lyon1.fr

Institut Lumière Matière, UMR5306, Université Lyon 1-CNRS, Université de Lyon, 69622 Villeurbanne, France

Phone : +33 472448046

Jean-Paul Rieu, jean-paul.rieu@univ-lyon1.fr

Institut Lumière Matière, UMR5306, Université Lyon 1-CNRS, Université de Lyon, 69622 Villeurbanne, France

Phone : +33 472432648

Vincent Calvez, vincent.calvez@math.cnrs.fr

Institut Camille Jordan, UMR5208, Université Lyon 1-CNRS, Université de Lyon, 69622 Villeurbanne, France.

Phone : +33 472431357

Abstract

It is well known that eukaryotic cells can sense oxygen (O_2) and adapt their metabolism accordingly. It is less known that they can also move towards regions of higher oxygen level (aerotaxis). Using a self-generated hypoxic assay, we show that the social amoeba *Dictyostelium discoideum* displays a spectacular aerotactic behavior. When a cell colony is covered by a coverglass, cells quickly consume the available O_2 and the ones close to the periphery move directionally outward forming a dense ring keeping a constant speed and density. To confirm that O_2 is the main molecular player in this seemingly collective process, we combined two technological developments, porphyrin based O_2 sensing films and microfluidic O_2 gradient generators. We showed that *Dictyostelium* cells exhibit aerotactic and aerokinetic (increased speed at low O_2) response in an extremely low range of O_2 concentration (0-1.5%) indicative of a very efficient detection mechanism. The various cell behaviors under self-generated or imposed O_2 gradients were modeled with a very satisfactory quantitative agreement using an *in silico* cellular Potts model built on experimental observations. This computational model was complemented with a parsimonious 'Go or Grow' partial differential equation (PDE) model. In both models, we found that the collective migration of a dense ring can be explained by the interplay between cell division and the modulation of aerotaxis, without the need for cell-cell communication.

Introduction

Oxygen is the main electron acceptor for aerobic organism to allow efficient ATP synthesis. This high-energy metabolic pathway has contributed to the emergence and diversification of multicellular organism (Chen et al., 2015). While high O_2 availability in the environment seems a given, its rapid local consumption can generate spatial and temporal gradients in many places, including within multicellular organism. Oxygen level and gradients are increasingly recognized as a central parameter in various physiopathological processes (Tonon et al., 2019), cancer and development. The well-known HIF (hypoxia inducible factor) pathway allows cells to regulate their behavior when exposed to hypoxia. At low O_2 levels, cells then accumulate HIFα leading to the expression of genes that support cell functions appropriate to hypoxia (Pugh & Ratcliffe, 2017).

Another strategy used by organisms facing severe oxygen conditions is to move away from hypoxic regions, a mechanism called aerotaxis first described in bacteria (Engelmann, 1881; Winn, Bourne, & Mitchell, 2013). Aerotaxis will occur at the interface between environments with different oxygen content, such as soil/air, water/air or even within eukaryotic multicellular organisms between different tissues (Lyons, Reinhard, & Planavsky, 2014). In such organisms, oxygen was proposed to be a morphogen as in placentation (Genbacev, Zhou, Ludlow, & Fisher, 1997) or a chemoattractant during sarcoma cell invasion (Lewis et al., 2016) but such studies are relatively scarce due to the difficultly to measure oxygen gradients *in vivo*.

Recently, it was demonstrated that after covering an epithelial cell colony by a coverglass non permeable to O_2, peripheral cells exhibit a strong outward directional migration to escape hypoxia from the center of the colony (Deygas et al., 2018). This is a striking example of collective response to a self-generated oxygen gradient. Self-generated chemoattractant gradients have been reported to trigger the dispersion of melanoma cells (Muinonen-Martin et al., 2014; Stuelten, 2017) or *Dictyostelium* cells (Tweedy, Susanto, & Insall, 2016) or the migration of the zebrafish lateral line primordium (Donà et al., 2013; Venkiteswaran et al., 2013). The mechanism is simple and very robust: the cell colony acts as a sink for the chemoattractant, removes it by degradation or uptake creating a gradient that, in turn, attracts the cells as long as the chemoattractant is present in the environment.

Dictyostelium discoideum (*Dd*) is an excellent model system to study the fairly virgin field of aerotaxis and of self-generated aerotaxis. *Dd* is an obligatory aerobic organism that requires at least 5% O_2 to grow at optimal exponential rate (Cotler & Raper, 1968; Sandonà, Gastaldello, Rizzuto, & Bisson, 1995) while slower growth can occur at 2% O_2. However, its ecological niche in the soil and around large amount of bacteria can result in reduced O_2 availability. During its multicellular motile stage, high

oxygen level is one of the signal used to trigger culmination of the migrating slug (Xu, Wang, Green, & West, 2012). For many years, *Dd* has been a classical organism to study chemotaxis and has emulated the development of many models of emergent and collective behavior since the seminal work of Keller and Segel (Hillen & Painter, 2009; Keller & Segel, 1970). An integrated approach combining biological methods (mutants), technological progress, and mathematical modeling is very valuable to tackle the issue of aerotaxis.

In this article, we study the influence of O_2 self-generated gradients on *Dd* cells. Using first a simple confinement assay, then microfluidic tools, original oxygen sensors and theoretical approaches, we show that oxygen self-generated gradients can direct a seemingly collective migration of a cell colony. Our results confirm the remarkable robustness and long-lasting effect of self-generated gradients in collective migration. This case where oxygen is the key driver also suggests that self-generated gradients are widespread and a possible important feature in multicellular morphogenesis.

Results

Confinement triggers formation and propagation of a self-sustained cell ring. To trigger hypoxia on a colony of *Dd* cells, we used a vertical confinement strategy (Deygas et al., 2018). A spot of cells with a radius of about 1mm was deposited and covered by a larger glass coverslip with a radius of 9mm. We measured the vertical confinement through confocal microscopy and found the height between the bottom of the plate and the coverslip to be 50μm (Fig. S1).

Using spots containing around 2,000 cells (initial density around 10^3 cells/mm^2), the formation of a dense ring of cells moving outwards was observed as quickly as 30min after initiation of the confinement (Fig. 1A and movie M1). This formation time however depended non-linearly on initial cell density (the denser, the faster, Fig. S2). Once triggered, this collective migration was self-maintained for tens of hours, even days and the ring could, at these points, span centimeters (Fig. 1B).

Notably, as the ring expanded outwards, it left a trail of cells behind. This led to the formation of a central zone populated by cells which didn't contribute to the migration of the ring (Fig. 1B) but were still alive and moving albeit a clear elongated phenotype resembling pre-aggregative *Dd* cells (Fig. 1C and movie M2). In comparison, cells in the ring or outside the colony were rounder, as usual vegetative cells (Delanoë-Ayari et al., 2008).

To study the properties of the ring, we computed density profiles using radial coordinates from the center of the colony to study cell density as a function of time and distance to the center (Fig. 1D-E). We found that after a transitory period corresponding to the ring passing through the initial spot, the density in the ring, its width and its speed all remained constant over long time scales (Fig. S3). The speed and density of the ring were found to be 1.2 ± 0.3 μm/min (mean±std, N=9) and 1.9 10^3 ± 0.3 10^3 cells/mm^2 (mean±std, N=4, *i.e.*, 4-fold higher than behind it, Fig. 1E) respectively. The density of cells left behind the ring was also found to remain constant after a transient regime (Fig. 1D). As the diameter of the ring increased over time, the absence of changes in morphology implies an increase of the number of cells and thus an important role of cell division.

Overall, this self-sustained ring propagation is very robust and a long lasting collective phenotype that can easily be triggered experimentally.

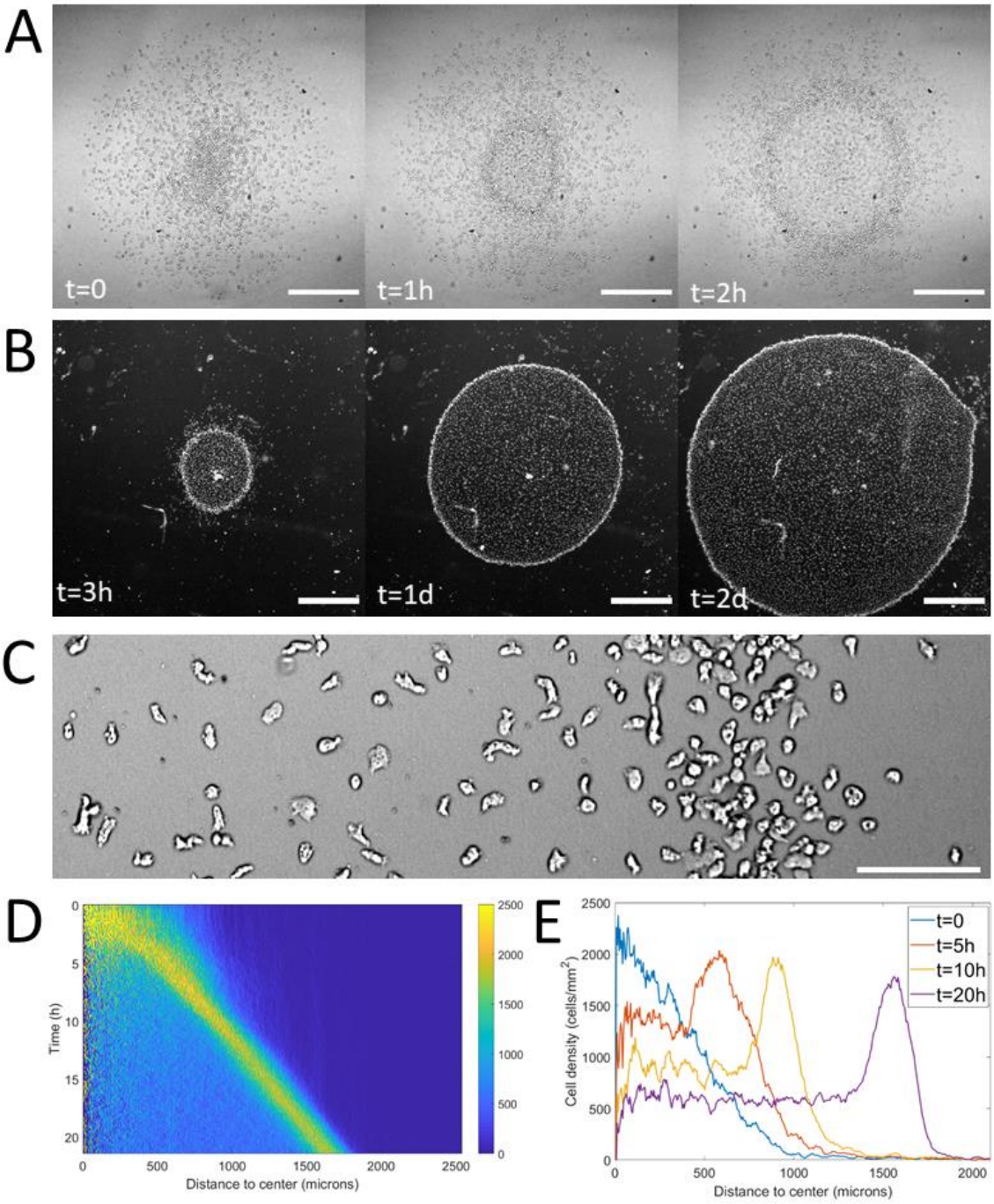

Fig1. *Formation and dynamics of a dense ring of cells after vertical confinement. (A) snapshots of early formation, scale bars: 500μm. (B) snapshots at longer times imaged under a binocular, scale bars: 1mm. (C) close up on a ring already formed moving rightward and showing different cellular shapes in the ring and behind it, scale bar: 100μm. (D) kymograph of cell density over 20h showing the formation and migration of the highly dense ring. (E) Cell density profiles in the radial direction at selected time points.*

Cell dynamics in different regions. Following the reported shape differences, we questioned how cells behaved dynamically in different regions. To do so, we performed higher resolution, higher frame rate experiments to allow cell tracking over times on the order of tens of minutes. Both the cell diffusion constant and instantaneous cell speeds were fairly constant throughout the entire colony (Fig. S4). Cell

138 diffusion was 28.2 $\pm$ 1.4 μm^2/min (N=3), comparable to our measurement of activity at very low oxygen
139 level in the microfluidic device (see below). To test the influence of motion bias, we projected cell
140 displacements on the radial direction and computed mean speeds in this direction as a function of
141 distance to the center. Random motion, either persistent or not, would lead to a null mean radial
142 displacement whereas biased migration would be revealed by positive (outward motion) or negative
143 (inward motion) values. Here, we found that significantly non-zero biases were observed only in a
144 region spanning the entire ring and a few tens of microns behind and in front of it with the strongest
145 positive biases found in the ring (Fig. S5).

146 Overall, our results show that the different regions defined by the ring and its dynamics can be
147 characterized in terms of cell behavior: (i) behind the ring in the hypoxic region: elongated shape,
148 normal speeds, and low bias; (ii) in the ring: round shape, normal speeds and high bias.

149 **Response of *Dd* cells to controlled oxygen gradients.** The spot assay is experimentally simple but is
150 not ideally suited to decipher the response of *Dd* cells to hypoxia since local concentrations and
151 gradients of oxygen are coupled to cell dynamics and thus very difficult to manipulate. We hence
152 designed a new double-layer PDMS microfluidic device allowing to quickly generate oxygen gradients
153 in a continuous, controlled manner (Fig. 2A). Briefly, cells were seeded homogenously within a media
154 channel positioned 500µm below two gas channels continuously perfused with pure nitrogen on one
155 side and air on the other. As PDMS is permeable to these gases, the gas flows imposed hypoxic
156 conditions on one side of the media channel while the other was kept at atmospheric oxygen
157 concentration. Of note, the distance between the two gas channels, thereafter called the gap, varied
158 from 0.5mm to 2mm in order to modify the steepness of the gradients in the median region of the
159 media channels (Fig. 2A and supplementary information).

160 To make sure that the gas flows were sufficient to maintain a constant O_2 distribution against leakages
161 and against small variation in the fabrication process, we also developed O_2 sensing films to be able to
162 experimentally measure O_2 profiles both in the microfluidic devices and in the spot assay. These films
163 consisted of porphyrin based O_2 sensors embedded in a layer of PDMS. As O_2 gets depleted, the
164 luminescence quenching of the porphyrin complex is reduced leading to an increase in fluorescence
165 intensity (Ungerböck, Charwat, Ertl, & Mayr, 2013). Quantitative oxygen measurements were then
166 extracted from this fluorescent signal using a Stern-Volmer equation (See supplementary information
167 and Figs. S6-S9 for details).

168 First, we observed the formation of a stable O_2 gradient in the devices closely resembling numerical
169 predictions with or without cells (Fig. 2B and Fig. S10-12).

170 We then turned our attention to the reaction of the cells to this external gradient. We first noticed
171 that depending on local O_2 concentrations, cell motility was remarkably different. Using cell tracking,
172 we found that cell trajectories seemed much longer and more biased in hypoxic regions (Fig. 2C). These
173 aerokinetic (large increase in cell activity) and aerotactic responses were confirmed by quantifying the
174 mean absolute distance travelled by cells (Fig. 2D top), or the mean distance projected along the
175 gradient direction (Fig. 2D bottom) in a given time as a function of position in the device (Fig. 2D).

176 The second important observation stemming from the microfluidic experiments is an accumulation of
177 cells at some midpoint within the cell channel (Fig. 2E). Naively, one could have expected cells to follow
178 the O_2 gradient over its entire span leading to an accumulation of all cells on the O_2 rich side of the
179 channel. This did not happen and, instead, cells seemed to stop responding to the gradient at a certain
180 point. Similarly, we observed a strong positive bias in hypoxic regions but the bias quickly fell to 0 as
181 cells moved to oxygen levels higher than about 2% (Fig. 2D), confirming that the observed cell
182 accumulation was a result of differential migration and not, for example, differential cell division. In
183 addition, if we inverted the gas channels halfway through the experiment, we observed that the cells
184 responded in around 15min (which is also the time needed to re-establish the gradient, see Fig. S11)

and showed the same behavior, albeit in reverse positions. We measured the bias for the different gaps and for the situation of reversed gradient and obtained a value of 1.1 ± 0.4 µm/min (N=6).

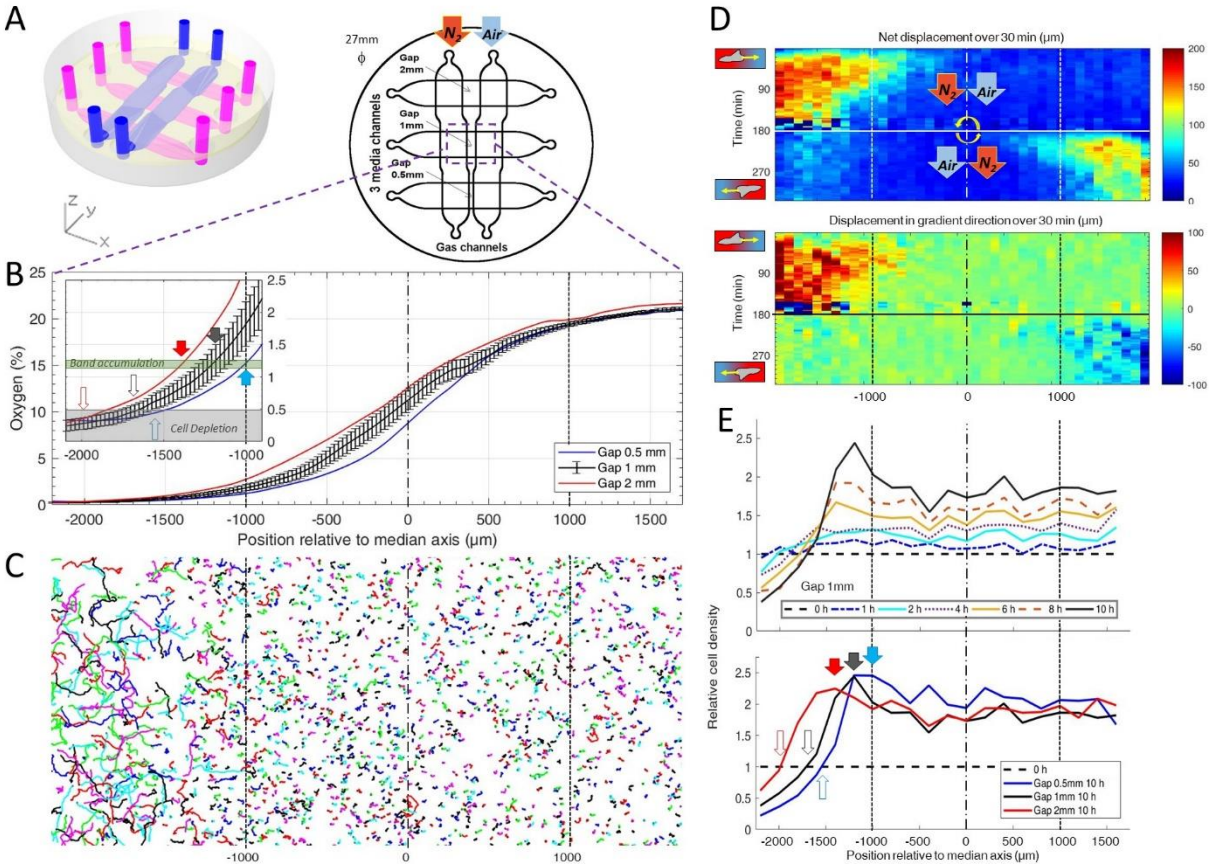

Fig. 2. *Dictyostelium single cells are attracted by an external O_2 gradient when O_2 level drops below 2%. (A) Schemes of the new double-layer PDMS microfluidic device allowing the control of the O_2 gradient by the separation distance (gap) between two gas channels located 0.5 mm above the three media channels and filled with pure nitrogen, and air (21% O_2). (B) Measured O_2 concentration profiles 30 min after N2-Air injection to the left and right channels respectively (0-21% gradient) as a function of the position along the media channel for the three gaps. Error bars (see supplementary information) are reported only for gap 1 mm for clarity. The inset shows the 0%-2.5% region under the nitrogen gas channel (arrows, see E). (C) Trajectories lasting 1 h between 3h and 4h after establishment of a 0-21% gradient. Cells are fast and directed toward the air side in the region beyond the -1000 µm limit (O_2<2%). (D) Cell net displacement over 30 min (end to end distance, top kymograph) and 30-min displacement projected along gradient direction (bottom kymograph). Cells are fast and directed toward O_2, where O_2<2%, within 15 min after 0-21% gradient establishment at t=0. At t=180 min, the gradient is reversed to 21-0% by permuting gas entries. Cells within 15 min again respond in the 0-2% region. (E) Relative cell density histogram (normalized to t=0 cell density) as a function of the position along media channel. Top panel: long term cell depletion for positions beyond -1600 µm (O_2<0.5%, see inset of B) and resulting accumulation at about -1200 µm for gap 1 mm channel. The overall relative cell density increase is due to cell divisions. Bottom panel: cell depletion and accumulation at 10 h for the three gaps. The empty and filled arrows pointing the limit of the depletion region, and max cell accumulation respectively are reported in the inset of B).*

Of note, the position at which cells accumulated and stopped responding to the gradient was still in the region were the gradient was constantly increasing. This led to the hypothesis that, in addition to

210 gradient strength, O_2 levels also play an important role in setting the strength of aerotaxis displayed
211 by *Dd* cells.

212 Furthermore, when we compared experiments performed with different gaps, we found that the
213 position of cell accumulation varied from one channel to another (Fig. 2E). However, our O_2 sensors
214 indicates that the accumulation occurred at a similar O_2 concentration of about 1% in all three channels
215 (inset of Fig. 2B) thus strongly hinting that the parameter controlling the aerotactic response was O_2
216 levels.

217 Overall, these experiments in controlled environments demonstrated two main features of the
218 response of *Dd* cells to hypoxia: a strong aerokinetic response and a positive aerotactic response, both
219 modulated by local O_2 levels regardless of the local gradient. These results reveal a subtle cross talk
220 between O_2 concentrations and gradients in defining cell properties and it would be very informative,
221 in the future, to study in details the reaction of *Dd* cells to various, well defined hypoxic environments
222 where O_2 concentrations and gradients can be independently varied.

223 **Coupled dynamics between oxygen profiles and collective motion.** Thanks to these results, we turned
224 our attention back to the collective migration of a ring of cells and asked whether similar aerotactic
225 behaviors were observed under self-generated gradients. To do so, we performed spot experiments
226 on the O_2 sensing films described above which allowed us to image, in parallel, cell behavior and O_2
227 distribution (Figs. 3A and S8, Movie M3).

228 In a first phase, preceding the formation of the ring, cell motion was limited and the structure of the
229 colony remained mostly unchanged. As O_2 was consumed by cells, depletion started in the center and
230 sharp gradients appeared at the edges of the colony (Fig. 3B-C).

231 Then, the ring formed and started moving outwards, O_2 depletion continued and the region of high O_2
232 gradients naturally started moving outwards (Fig. 3B). At this point, coupled dynamics between the
233 cells and the O_2 distribution appeared and we observed that the position of the ring closely followed
234 the dynamics of the O_2 field (Fig. 3D), *i.e.* a constant concentration of oxygen of less than 1% (Fig. 3C).

235 In the process, three distinct regions were created. Behind the ring, O_2 was completely depleted and
236 thus no gradient was visible. In front of the ring, the O_2 concentration remained high with high
237 gradients. Finally, in the ring region, O_2 was low (<1%) and the gradients were strong. Based on our
238 results in externally imposed gradients, we would thus expect cells to present a positive aerotactic bias
239 mostly in the ring region which is indeed what we observed (Fig S5).

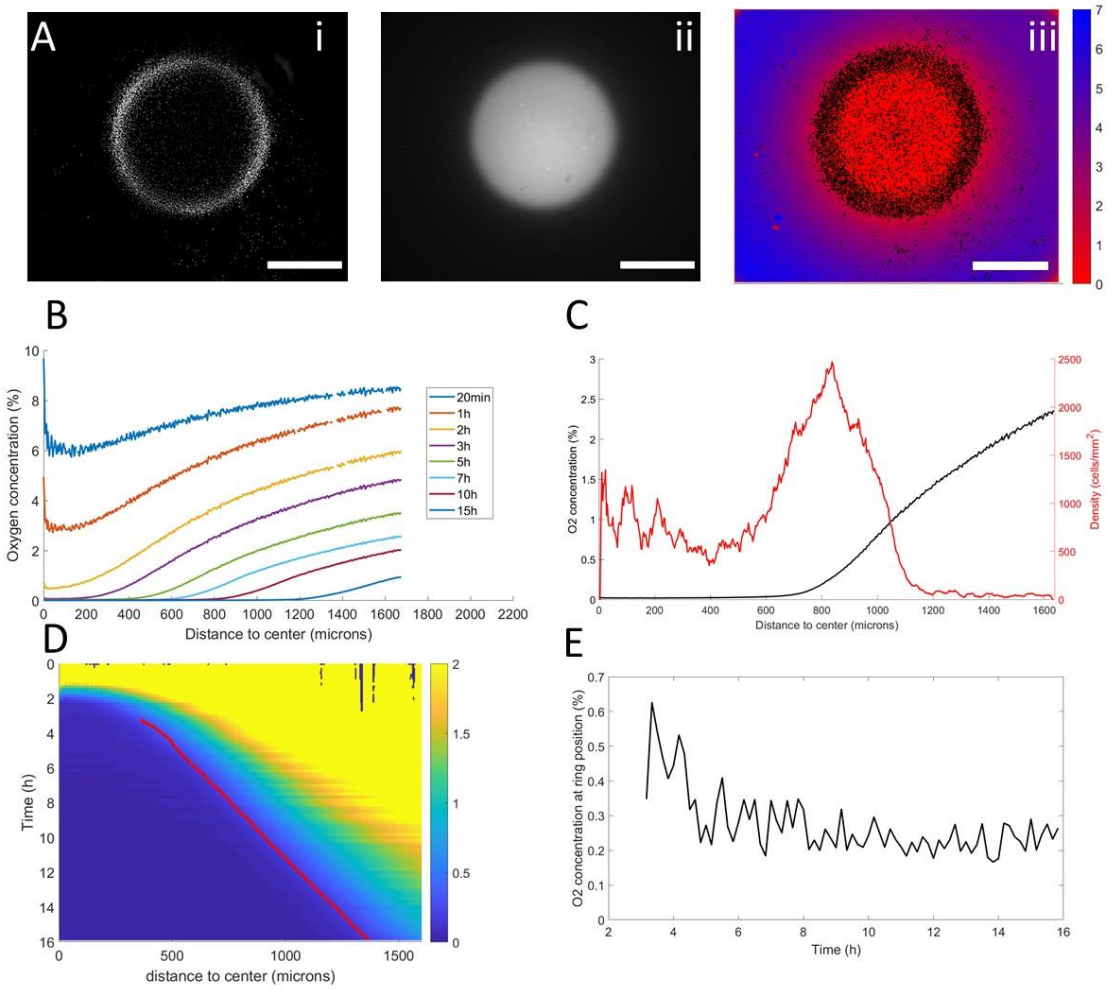

Fig3. *Interplay between ring dynamics and O_2 profiles. (A) i: treated image showing cell distribution at t=10h, ii: raw fluorescent signal indicative of strong O_2 depletion, iii: reconstructed image showing the center of mass of all detected cells and quantitative O_2 profiles (colorbar, in % of O_2), scale bars: 1mm. (B) O_2 profiles averaged over all angles and shown at different times. (C) radial profile of cell density and O_2 concentration at t=10h showing the position of the ring relative to the O_2 profile. (D) kymograph of O_2 concentration (colorbar in %) with the position of the ring represented as a red line. The colormap is limited to the 0-2% range for readability but earlier time points show concentrations higher than the 2% limit. (E) O_2 concentration as measured at the position of the ring as a function of time showing that the ring is indeed following a constant concentration after a transitory period.*

Minimal cellular Potts Model. Based on these experimental results, we then asked whether this subtle response of *Dd* cells to complex oxygen environments was sufficient to explain the emergence of a highly stable, self-maintained collective phenomenon. To do so, we developed cellular Potts models based on experimental observations and tested whether they could reproduce the observed cell dynamics. Briefly, the ingredient underlying the model are as follows (details can be found in the supplementary information). First, all cells consume the oxygen that is locally available at a known rate (Torija et al., 2006). Cell activity increases at low O_2. Cells respond positively to O_2 gradients with a modulation of the strength of this aerotaxis based on local O_2 concentrations, as observed in our microfluidic experiments. Finally, all cells can divide. Of note, all parameters were scaled so that both time and length scales in the Potts models are linked to experimental times and lengths (see Supplementary Information).

Although this model is based on experimental evidence, some of its parameters are not directly related to easily measurable biological properties. Therefore, we decided to fit our parameters to reproduce as faithfully as possible the results of our microfluidic experiments. Through a trial and error procedure, we managed to reproduce these results qualitatively and quantitatively (Movie M4) in terms of collective behavior, cell accumulation, and individual cell behavior (Fig. S13).

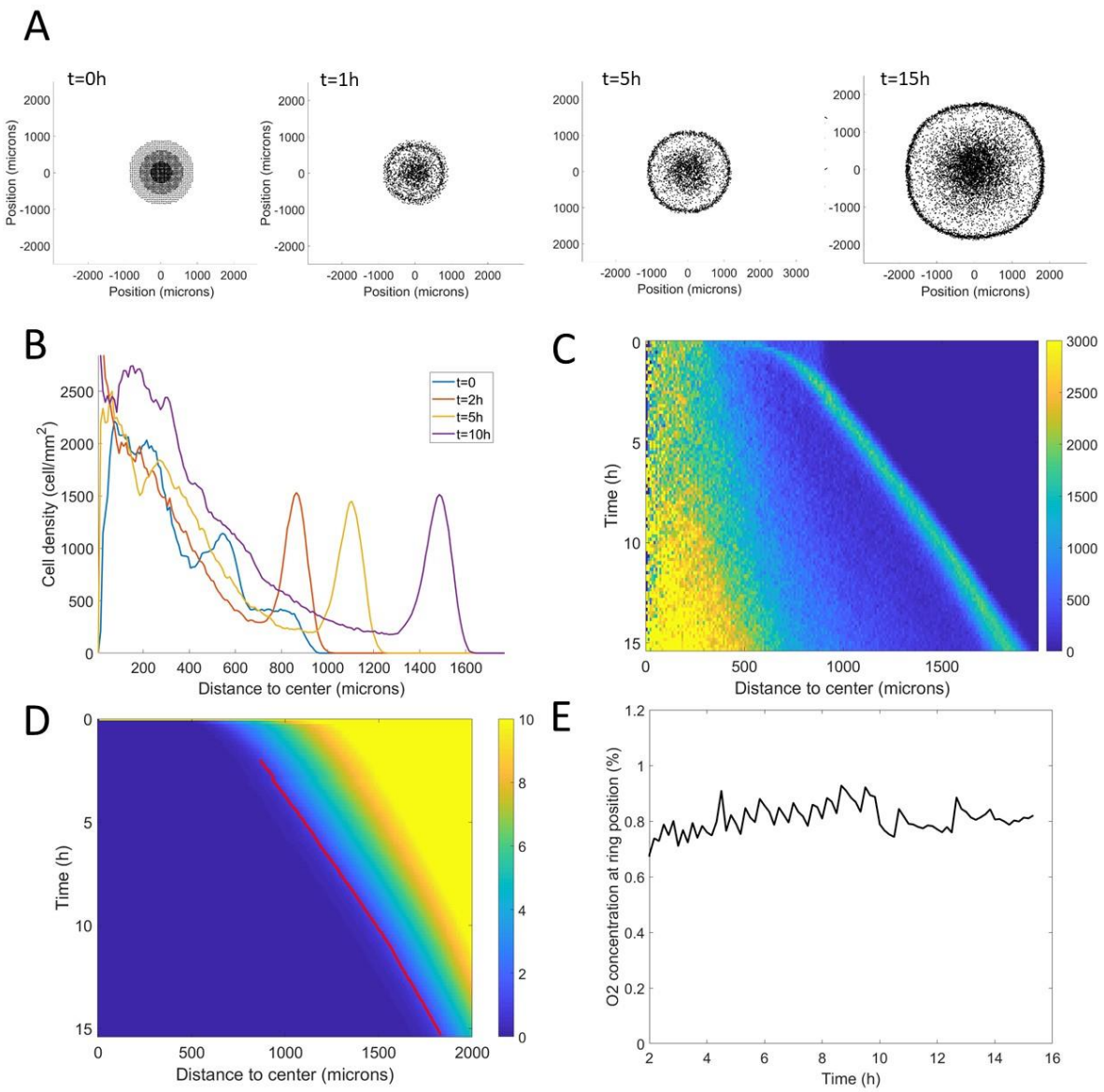

Fig. 4. Minimal Potts model of ring formation and migration. (A) Snapshots of a simulated colony of cells showing the formation of highly dense ring of cells. (B) Cell density profiles averaged over all angles for four different times. (C) Corresponding kymograph of cell density (colorbar in cells/mm^2) as a function of time and distance to the center. Quantification in terms of microns and hours is described in the supplementary information. (D) Kymograph of O_2 concentration (colorbar in %) with the position of the ring represented as a red line. The colormap is limited to the 0-10% range for readability but earlier time points show concentrations higher than the 10% limit. (E) O_2 concentration at the ring position as a function of time showing that, here too, the ring follows a constant O_2 concentration.

We then applied this model and added O_2 consumption by cells, with initial conditions mimicking our spot assay and other ingredients mimicking the vertical confinement (see Supplementary Methods). We observed the rapid formation and migration of a ring (Fig. 4A-B, Movie M5). This ring was remarkably similar to that observed in experiments. In particular, we found its speed to be constant after an initial transitory period (Fig. 4C, Fig. S14). This speed was also comparable to experimental ones. Similarly, the morphology of these simulated rings was constant over time with a fixed cell density and width (Fig. S14). Finally, cell behavior was qualitatively well reproduced by this model (Fig. S15) with the exception of a remaining dense core of cells in the center which disappeared if cell consumption (or initial cell density) was reduced (see Fig 5A).

In terms of coupled dynamics between cell density and O_2 profiles, we found here too that the driving force behind this collective phenomenon was the fact that the ring followed a constant O_2 concentration (Fig. 4D-E).

We then asked what were the key ingredients in the model to trigger this phenomenon, a question we explored by tuning our original Potts model. We started by dividing cell consumption of oxygen by a factor of 3 (Fig. 5A) and found that it didn't significantly change the ring speed but could change the aspect of cell density in the central region. We then turned our attention to other key elements in the model.

If we turned off cell division in our models, the formation of the ring was mostly unchanged but after a short time, the ring started slowing down and even stopped as cell density was no longer sufficient to reach highly hypoxic conditions (comparing Fig5 A and B). Second, we asked whether the observed and modelled aerokinesis was necessary to reproduce the collective migration. We found that it wasn't as models ran at different effective temperatures applied to all cells regardless of local O_2 concentrations, all showed qualitatively similar behavior (see for example Fig. 5C). Of note though, lower effective temperatures led to less dense rings as fewer cells were able to start in the ring (Fig. S16). Finally, we found that modulation of aerotaxis by local O_2 concentrations was essential. Indeed, as we increased the range of O_2 concentration at which aerotaxis is at play (Fig 5G-H), we found that forming rings became wider and less dense (Fig. 5 D-E) to the point where no actual ring could be distinguished if aerotaxis was kept constant for all cells (Fig. 5I).

These numerical simulations based on cellular Potts models provide a good intuition of the phenomenon and reveal that cell division and aerotactic modulation are the two key ingredients to reproduce the ring of cells. They fall short however of giving an in-depth quantitative description because they rely on many parameters and are not amenable to theoretical analysis *per se*.

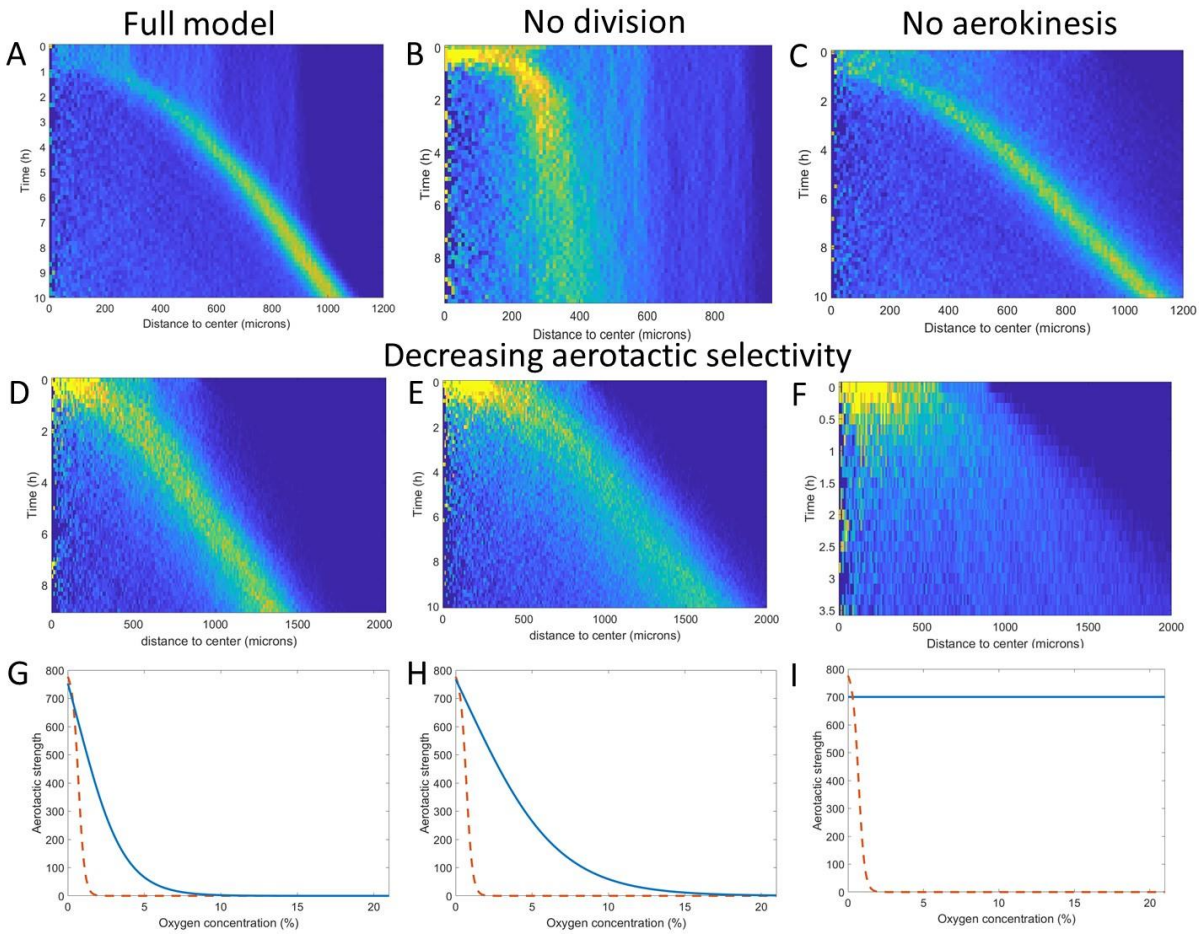

Fig. 5. *Key ingredients of the Potts model by density kymograph (DK) evaluation. (A) DK for the full model with reduced oxygen consumption as a basis for comparison. (B) DK in the absence of cell division, note the difference in length scale showing a clear limitation of motion in that case. (C) DK in the absence of aerokinesis (cell activity is not modulated by local oxygen concentrations). (D) DK with a modulation of aerotactic strength as shown in (G), note the wider ring. (E) DK with a modulation of aerotactic strength as shown in (H). (F) DK with a modulation of aerotactic strength as shown in (I), no ring appears and cells quickly migrate outwards as shown by the difference in time scales. (G-I) Three different aerotactic modulations, in blue, compared to the one used in the full model, shown in (A), drawn here as a red dashed line.*

Single-threshold 'Go or Grow' model. For the above mentioned reasons, we developed a simple, yet original, model based on the two key ingredients while keeping it analytically solvable. Cell density is treated as a continuous field, O_2 consumption and diffusion are included. Cells have two distinct behaviors, depending on the O_2 concentration. Below a certain threshold C_0 cells move preferentially upward the oxygen gradient, with constant advection speed a_0, but they cannot divide. Above the same threshold they divide and move randomly without directional bias. We refer to these behaviors as respectively *go* or *grow*. We thereby revisit the 'Go or Grow' model for glioma cells (Hatzikirou, Basanta, Simon, Schaller, & Deutsch, 2012) with the transition between division and directional motion being mediated by oxygen levels rather than cell density. This model is meant to 1- demonstrate that these ingredients suffice to trigger a collective motion and 2- determine the relative contributions of division and aerotaxis on the speed of the ring.

For the sake of simplicity and its relevance for the study of planar front propagation, we restrict ourselves to the one-dimensional case, ignoring curvature effects. Our 'Go or Grow' model is a piecewise constant reaction-advection-diffusion equation:

[EQ1] $$\frac{\partial \rho}{\partial t} = D\frac{\partial^2 \rho}{\partial x^2} - \frac{\partial}{\partial x}(a(C)sign(\partial_x C)\rho) + r(C)\rho, with$$

$$a(C) = \begin{Bmatrix} 0 if C > C_0 \\ a_0 if C < C_0 \end{Bmatrix}$$

$$r(C) = \{ \begin{matrix} r_0 if C > C_0 \\ 0 if C < C_0 \end{matrix} \}$$

$a(C)sign(\partial_x C)$ corresponds to the aerotactic advection speed and $r(C)$ to the cell division rate.

Oxygen is subject to a simple diffusion-consumption equation, with b the constant consumption rate of oxygen per cell:

[EQ2] $$\frac{\partial C}{\partial t} = D_{oxy}\frac{\partial^2 C}{\partial x^2} - b\rho C$$

The coupling goes through the location of the oxygen threshold C_0.

We investigated the existence of traveling wave profiles at some unknown speed $\sigma > 0$. The equation for the one-dimensional profile, being stationary in the moving frame $z = x - \sigma t$, is:

[EQ3] $$-\sigma\frac{\partial \rho}{\partial z} = D\frac{\partial^2 \rho}{\partial z^2} - \frac{\partial}{\partial z}(a(C)\rho) + r(C)\rho$$

Interestingly enough, it admits explicit solutions, whose speed does not involve the dynamics of oxygen consumption. This yields the following formula for the wave speed (Fig. 6A):

[EQ4] $$\sigma = \begin{Bmatrix} a_0 + \frac{r_0 D}{a_0} if a_0 > \sqrt{r_0 D} \\ 2\sqrt{r_0 D} if a_0 \leq \sqrt{r_0 D} \end{Bmatrix}$$

To the best of our knowledge, this analytical formula is new and captures basic features of a wave under a single self-generated gradient.

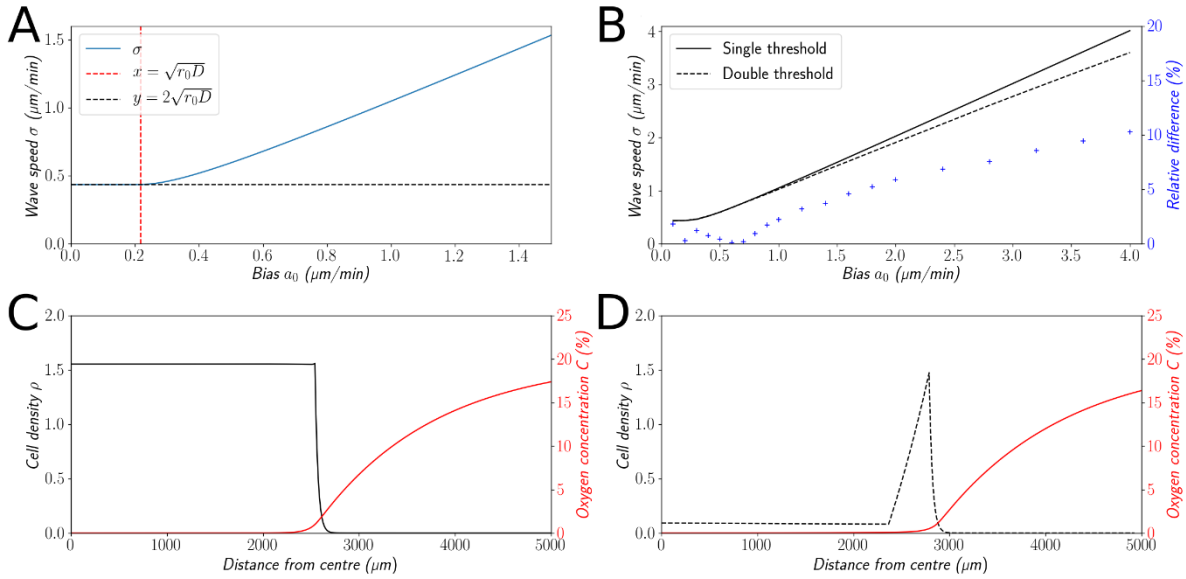

Fig. 6. *Simple 'Go or Grow' model. (A): Illustration of wave speed given by EQ4. (B): Comparison of wave speeds for the single-threshold and the double-threshold models (solid and dotted lines respectively) and relative difference between the two models (crosses). (C): Traveling wave profile of cell density and O_2 concentration for the single-threshold model (EQ1 & EQ2). (D): Traveling wave profile of cell density and O_2 concentration for the double-threshold model. In both cases, thresholds coincide with points of sharp transitions in the profiles.*

Double-threshold 'Go or Grow' model and variations. The cell density profile (Fig. 6C) of the 'Go or Grow' model EQ1 is clearly not in agreement with the observation of a dense ring of cells followed by an expanding zone at lower density (Fig. 1). Yet through elementary structural variations of the model, we obtained cell density profiles more similar to experimental ones, without significant alterations to the quantitative and qualitative conclusions.

First, we made the hypothesis of a second oxygen threshold $C_0{}' < C_0$, below which cells are not sensitive to gradients any longer. Notably, this model exhibits traveling wave profiles with a dense ring of cells, leaving behind a spatially uniform low cell density (Fig. 6D) much more similar to experimental observations. An exhaustive analytical investigation of this model seems out of reach, but we analyzed it numerically. The speed of the numerical wave remained close to the value given by formula EQ4 (at most 10% of relative difference, Fig. 6B). Intuitively, the main contribution to the collective speed is the strong bias inside the ring at intermediate levels of O_2, whereas cells at levels below the second threshold $C_0{}'$, where the dynamics of both models diverge, do not contribute much to the collective speed.

Second, we investigated more complex responses of cells to oxygen levels (Fig. S17). We assumed a continuous dependency of the bias to the O_2 concentration, rather than a discontinuous switch as in EQ1. In parallel, we assumed a continuous dependency of the division rate. The conclusions remained qualitatively and quantitatively the same (Fig. S17).

Therefore, properties of the 'Go or Grow' model, which we can prove analytically, like formula EQ4 and features discussed below, appear to be robust to substantial variations.

Comparison with the Fisher-KPP reaction-diffusion equation. The Fisher-KPP equation is a standard model for the linear expansion of populations (Fisher, 1937; Kolmogorov, Petrovskii, & Piskunov, 1937). It describes front propagation under the combined effects of diffusion and growth. The wave

speed of our 'Go or Grow' model coincides with Fisher's speed, i.e. $\sigma = 2\sqrt{r_0 D}$, in the regime of small bias ($a_0 \leqslant \sqrt{r_0 D}$). This is the signature of a *pulled wave*, meaning that the propagation is driven by the division and motion of cells at the edge of the front, with negligible contribution from the bulk. In contrast, when the bias is large ($a_0 > \sqrt{r_0 D}$) then the wave speed in [EQ4] is greater than Fisher's speed. This is the signature of a *pushed wave*, meaning that there is a significant contribution from the bulk to the net propagation, see (Birzu, Hallatschek, & Korolev, 2018) for recent insights about the dichotomy between pulled and pushed waves.

In order to explore this dichotomy between pulled and pushed waves, we used the framework of neutral labeling (Roques, Garnier, Hamel, & Klein, 2012) in the context of PDE models. We colored fractions of the density profile to mimic labeling of cells with two colors. Then, we followed numerically the dynamics of these fractions, and quantified the mixing of the two colors. Our results are in perfect agreement with (Roques et al., 2012), extending their results beyond classical reaction-diffusion equations, including advection (see supplementary information section 3.2). In the case of large bias (Fig. 7A-C) the wave is pushed and the profile is a perfect mixture of blue and yellow cells at long time. Contrarily, the wave is pulled in the regime of small bias: only cells that were already initially in the front, here colored in blue (Fig. 7B-D), are conserved in the front, whilst yellow cells at the back cannot catch up with the front.

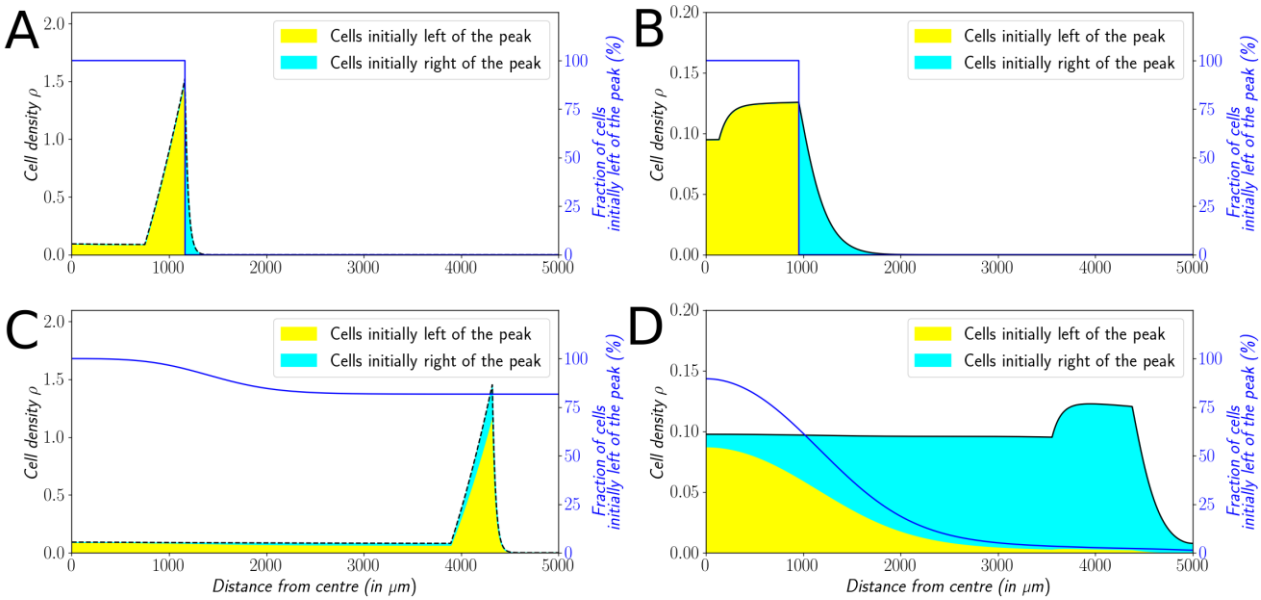

Fig. 7. *Classification of the expansion type. Cells initially on the left-hand side or right-hand side of the peak get labeled differently (A&B). The labeling is neutral and does not change the dynamics of the cells. We let evolve the two colored population for some time and observe the mixing of the colors (C&D). (A&C) : With* $a_0 = 1\mu m \cdot s^{-1}$*, the wave is pushed wave and after some time the front undergoes a spatially uniform mixing. (B&D) : With* $a_0 = 0.1\mu m \cdot s^{-1}$*, the wave is pulled and only the fraction initially in the front is conserved in the front.*

In the absence of associated experimental data, we explored the cellular Potts model with such neutral labeling. The results were in agreement with the PDE simulations (Fig. S18) showing a clear, rapid mixing of the two cell populations under the propagation of a pushed wave.

Relative contribution of growth and aerotactic bias to the collective motion in experiments. In [EQ4] we see that growth contributes to the wave speed either via the geometric mean of growth rate r_0 and diffusion coefficient D, in the case of small bias, or via a linear term supplementing the advection speed a_0 for large bias. As a rough approximation with $a_0 = 1\mu m \cdot min^{-1}$, assuming a doubling time of 8h for *Dd* cells and $D = 30\mu m^2 \cdot min^{-1}$, we are clearly in the case of large bias ($\sqrt{r_0 D} = 0.21\mu m \cdot min^{-1}$) and EQ4 yields $\sigma = 1.04\mu m \cdot min^{-1}$. The exact contribution of growth depends on the variations of the model (numerical explorations have shown contributions of growth of at most 20%, see Supplementary Information), yet even with this elementary reasoning we were able to estimate that growth contributes only up to a small fraction to the overall speed.

Overall, the invesvestigation of the 'Go or Grow' model and its variations show that the ring speed is mainly the outcome of the interplay between cell division and aerotaxis.

Discussion

While aerotaxis is well established for bacteria, its role is often invoked in multicellular organisms to explain various processes in development or cancer progression, but very few *in vitro* studies were conducted to prove it is an efficient and operating mechanism or to understand the molecular mechanisms at play during aerotaxis. Deygas et al. showed that confined epithelial colonies may trigger a self-generated O_2 gradient and an aerotactic indirect response through a secondary ROS self-generated gradient (Deygas et al., 2018). Gilkes et al. showed that hypoxia enhances MDA-MB231 breast cancer cell motility through an increased activity of HIFs (Gilkes et al., 2014). HIFs activate transcription of the Rho family member RHOA and Rho kinase 1 (ROCK1) genes, leading to cytoskeletal changes, focal adhesion formation and actomyosin contractions that underlie the invasive cancer cell phenotype. This study suggests a role for aerotaxis in tumor escape, but it only demonstrates aerokinesis as O_2 gradients were not imposed to probe a directed migration toward O_2. Using a microfluidic device, the same cancer cell line was submitted to various oxygen levels as well as oxygen gradients(Koens et al., 2020) but the observed aerotactic response was not clear.
By contrast, the experimental results presented here with *Dd* show a strong response to hypoxia. Within 15min, cells exhibit an aerokinetic and aerotactic response when exposed to externally imposed O_2 gradients (Fig. 2). Self-generated O_2 gradients are produced within 20 min (Fig. 3 and Fig. S2). But this cellular response is within the equilibration time of the oxygen distribution (Fig. S11). Hence we can consider the cellular response as almost instantaneous with *Dd*. The difference with previously studied cells is probably due to the extreme plasticity of the rapidly moving amoeboid cells (*Dd*) and their almost adhesion independent migration mechanism (Friedl, Borgmann, & Bröcker, 2001) while mesenchymal cancer cells move slower by coordinating cytoskeleton forces and focal adhesion (Palecek, Loftust, Ginsberg, Lauffenburger, & Horwitz, 1997).
The quick response of *Dd* in directed migration assays has been largely exploited to decipher the molecular mechanisms at play during chemotaxis (Nakajima, Ishihara, Imoto, & Sawai, 2014). The molecular mechanisms used for O_2 sensing and its transduction into cellular response are for the moment unknown but we can expect that the O_2 molecular sensors modulate cytoskeleton organization, particularly localized actin polymerization/depolymerization through some of the molecular components involved in classical chemotaxis toward folate or cAMP (Pan, Xu, Chen, & Jin, 2016; Van Haastert, Keizer-Gunnink, & Kortholt, 2017). However, new and unexpected mechanisms cannot be excluded.
The finding that migrating cells can influence the direction of their own migration by building chemoattractant gradients is not new but it was only recently reported for various systems (Stuelten, 2017): melanoma cells that break down lysophosphatidic acid (LPA) and generate a LPA gradient in the vicinity of the tumor (Muinonen-Martin et al., 2014), *Dd* colonies that generate folate gradients (Tweedy et al., 2016) or for the migration of the zebrafish lateral line primordium through a self-generated chemokine gradient (Donà et al., 2013; Venkiteswaran et al., 2013). The dispersal of melanoma cells is particularly instructive. The stroma surrounding the tumor acts as a source of LPA. The tumor cells act as a sink for LPA. As long as LPA is present in the environment a steady wave of

466 migrating melanoma cells propagates away from the initial tumor over long distances and long time
467 periods.
468 The self-generated LPA (melanoma) and folate (*Dd*) gradients were modeled with a simple numerical
469 model that was able to predict the steady wave. In particular, it predicted an invasive front where cells
470 are exposed to a steep chemoattractant gradient, followed by a 'trailing end' where the gradient is
471 shallow and fewer cells migrate with poor directionality(Tweedy & Insall, 2020). It also predicted that
472 the wave may have a less marked front, and/or a smaller speed, or even vanishes if the cell density
473 was too low due to insufficient chemoattractant removal. All these features are surprisingly similar to
474 our experimental measurements of cell density and O_2 profiles (Fig. 1E, Fig. 3C). The atmospheric O_2
475 that diffuses through the culture medium and eventually the plastic surfaces is the chemoattractant.
476 The O_2 consumption triggers hypoxia that in turn generate an aerotactic response toward O_2 in a very
477 narrow range of O_2 concentrations (0-1.5%) (Fig. 3C). The exact value of the lower O_2 threshold value
478 will deserve future investigations. The exact nature of the cellular response at these extremely low O_2
479 levels, and in a very shallow gradient, also has yet to be clarified.
480 Our different models unveil a set of basic assumptions which are sufficient for collective motion of
481 cells without cell-cell interactions (attractive or otherwise), in contrast with (Saragosti et al., 2011). Cell
482 growth is necessary to produce a long-standing wave without any damping effect. However, it may not
483 be the main contribution in the wave speed, depending on the relative ratio between directional
484 motion (the bias a_0), and reaction-diffusion (the Fisher half-speed $\sqrt{r_0 D}$). In the case where the
485 former is greater than the latter, the wave is due to the combination of growth and directional motion
486 and it is pushed. This result differs particularly from the Fisher equation with constant advection
487 (meaning with uniform migration and division) where the wave speed is $a_0 + 2\sqrt{r_0 D}$ and the wave is
488 pulled. In the experiments under study, we estimate directional motion to contribute the most to the
489 cell speed, ruling out the possibility of seeing a pulled wave driven by cell division and diffusion at the
490 edge of the front.

491 In conclusion, we demonstrate the remarkable stability of collective motion driven by self-generated
492 gradients through depletion of an attractant. Through coupled dynamics, these gradients give rise to
493 long lasting, communication-free migrations of entire colonies of cells which are important both from
494 ecological and developmental points of view. In the case presented here where oxygen plays the role
495 of the depleted attractant, this could prove to be a very general mechanism as oxygen is ubiquitous
496 and always consumed by cells.

497

498 # Methods

499 **Cell preparation.** Cells were grown in HL5 media at 22°C with shaking at 180 rpm for oxygenation
500 (Sussman, 1987). Exponentially growing cells were harvested, counted to adjust cell density at typically
501 2000 cells/μL. For the spot assay, 1 μL of cell suspension was carefully deposited on a dry surface (6
502 wells plastic plates or PDMS for oxygen sensing) and incubated for 5 to 7 minutes in humid
503 atmosphere. 2 ml HL5 was slowly added to avoid detaching cells and a wetted coverslip was then
504 deposited on top of the micro-colony. The micro-colony was then observed under video-microscope
505 and analysed with ImageJ and Matlab (see supplementary information).

506 **Microfluidic devices and O_2 sensing films.** Using soft lithography, we manufactured a double layer
507 PDMS microfluidic device to control a O_2 gradient along the cell-media channel. The gradient is
508 established within 15 min. We also developed coverglass coated with a thin layer of PDMS with
509 porphyrin embedded: the quenching by O_2 of the porphyrin luminescence enables the direct
510 measurement of the O_2 concentration from a proper calibration of the fluorescence intensity (details
511 are given in the supplementary information).

512 **Potts models.** Potts model simulations were run using CompuCell3D (Swat et al., 2012) with a mix of
513 prebuilt modules and home-made Python steppables in particular to implement the modulation of

aerotactic strength by local oxygen levels. Most parameters were fitted to experimental measurements and both time and length scales were also adapted to achieve quantitative simulations. Full details of the model can be found in Supplementary Methods and full codes are available upon request to the corresponding authors.

Go or grow model and simulations. Both diffusion equations EQ1&EQ2 were discretized through a time-backward space-centered difference scheme with an upwind discretization for the advection operator:

$$\frac{\rho_i^{n+\frac{1}{2}}-\rho_i^{n-\frac{1}{2}}}{\Delta t} - D\frac{\rho_{i-1}^{n+\frac{1}{2}}-2\rho_i^{n+\frac{1}{2}}+\rho_{i+1}^{n+\frac{1}{2}}}{\Delta x^2} + \frac{1}{\Delta x}\cdot\left\{\begin{matrix} a_i^n\rho_i^{n+\frac{1}{2}} - a_{i-1}^n\rho_{i-1}^{n+\frac{1}{2}} if C_i^n \geq C_{i-1}^n \\ a_i^n\rho_i^{n+\frac{1}{2}} - a_{i+1}^n\rho_{i+1}^{n+\frac{1}{2}} if C_i^n < C_{i-1}^n \end{matrix}\right\} = r_i^n\rho_i^{n+\frac{1}{2}}, \text{ where}$$

$$a_i^n = a(C_i^n), r_i^n = r(C_i^n)$$

$$\frac{C_i^{n+1}-C_i^n}{\Delta t} - D_{oxy}\frac{C_{i-1}^{n+1}-2C_i^{n+1}+C_{i+1}^{n+1}}{\Delta x^2} = -b\rho_i^{n+\frac{1}{2}}C_i^{n+1}$$

The schemes were coded in Python language. All simulations of EQ1&EQ2 shown in this article were carried out with a mesh size $\Delta t = 1min$ and $\Delta x = 1\mu m$. The values used for the constants are : $D = 30\mu m^2 \cdot min^{-1}$, $C_0 = 1\%$, $C_0{}' = 0.1\%$, $D_{oxy} = 1300\mu m^2 \cdot s^{-1}$, $r_0 = ln\,2/480\,min^{-1}$and $b = 0.1O_2\%min^{-1}cell^{-1}$.

Acknowledgments

We thank R. Fulcrand for his expert help in microfabrication; G. Torch, C. Zoude, G. Simon and A. Piednoir for technical assistance. This study was supported by the CNRS - Mission pour les Initiatives Transverses et Interdisciplinaires – « Défi Modélisation du vivant - 2019», by the GDR ImaBio (AMI fellowship) and by the IFS LyC Collaborative Research Project 2019 (Tohoku University). S. Hirose was supported by the STARMAJ Program (France-Japan: Research Internships for Master's Students, Université de Lyon) and K. Funamoto by the CNRS (invited researcher position). This project has received funding from the European Research Council (ERC) under the European Union's Horizon 2020 research and innovation programme (grant agreement No 639638 to V.Calvez).

Author contributions

KF, VC, PG, IM, CA, JPR and OCE designed the research. PG, IM, BA, CA and JPR adapted the spot assays The microfluidic chambers were developed by JPR, KF and SH. Oxygen sensors were developed and manufactured by JPR, OCE, IM, KF and SH. OCE, BA, SH, KF, CA and JPR performed experiments. MD, VC and OCE performed numerical simulations and calculations. OCE, JPR, CA, MD and VC wrote the paper and all authors edited the manuscript.

References

Birzu, G., Hallatschek, O., & Korolev, K. S. (2018). Fluctuations uncover a distinct class of traveling waves. *Proceedings of the National Academy of Sciences of the United States of America*, *115*(16), E3645–E3654. https://doi.org/10.1073/pnas.1715737115

Chen, X., Ling, H., Vance, D., Shields-zhou, G. A., Zhu, M., Poulton, S. W., … Archer, C. (2015).

Rise to modern levels of ocean oxygenation coincided with the Cambrian radiation of animals. *Nature Communications*, *6*(May), 7142. https://doi.org/10.1038/ncomms8142

Cotler, D. A., & Raper, K. B. (1968). Properties of Germinating Spores of Dictyostelium discoideum. *Journal of Bacteriology*, *96*(5), 1680–1689.

Delanoë-Ayari, H., Iwaya, S., Maeda, Y. T., Inose, J., Rivière, C., Sano, M., & Rieu, J.-P. (2008). Changes in the magnitude and distribution of forces at different dictyostelium developmental stages. *Cell Motility and the Cytoskeleton*, *65*(4), 314–331. https://doi.org/10.1002/cm.20262

Deygas, M., Gadet, R., Gillet, G., Rimokh, R., Gonzalo, P., & Mikaelian, I. (2018). Redox regulation of EGFR steers migration of hypoxic mammary cells towards oxygen. *Nature Communications*, *9*(1), 4545. https://doi.org/10.1038/s41467-018-06988-3

Donà, E., Barry, J. D., Valentin, G., Quirin, C., Khmelinskii, A., Kunze, A., … Gilmour, D. (2013). Directional tissue migration through a self-generated chemokine gradient. *Nature*, *503*(7475), 285–289. https://doi.org/10.1038/nature12635

Engelmann, T. W. (1881). Neue methode zur untersuchung der sauerstoffausscheidung pflanzlicher und tierischer organismen (New method for investigation of oxygen-searching plant and animal organisms). *Pflugers Arch. Gesammte Physiol.*, *25*, 285–292.

Fisher, R. A. (1937). The wave of advance of advantageous genes. *Annals of Eugenics*, *7*(4), 355–369. https://doi.org/10.1111/j.1469-1809.1937.tb02153.x

Friedl, P., Borgmann, S., & Bröcker, E. B. (2001). Amoeboid leukocyte crawling through extracellular matrix: lessons from the Dictyostelium paradigm of cell movement. *Journal of Leukocyte Biology*, *70*(4), 491–509. https://doi.org/10.1189/jlb.70.4.491

Genbacev, O., Zhou, Y., Ludlow, J. W., & Fisher, S. J. (1997). Regulation of human placental development by oxygen tension. *Science*, *277*(5332), 1669–1672. https://doi.org/10.1126/science.277.5332.1669

Gilkes, D. M., Xiang, L., Lee, S. J., Chaturvedi, P., Hubbi, M. E., Wirtz, D., & Semenza, G. L. (2014). Hypoxia-inducible factors mediate coordinated RhoA-ROCK1 expression and signaling in breast cancer cells. *Proceedings of the National Academy of Sciences of the United States of America*, *111*(3), E384. https://doi.org/10.1073/pnas.1321510111

Hatzikirou, H., Basanta, D., Simon, M., Schaller, K., & Deutsch, A. (2012). “Go or grow”: The key to the emergence of invasion in tumour progression? *Mathematical Medicine and Biology*, *29*(1), 49–65. https://doi.org/10.1093/imammb/dqq011

Hillen, T., & Painter, K. J. (2009, January 15). A user’s guide to PDE models for chemotaxis. *Journal of Mathematical Biology*. Springer. https://doi.org/10.1007/s00285-008-0201-3

Keller, E. F., & Segel, L. A. (1970). Initiation of slime mold aggregation viewed as an instability. *Journal of Theoretical Biology*, *26*(3), 399–415. https://doi.org/10.1016/0022-5193(70)90092-5

Koens, R., Tabata, Y., Serrano, J. C., Aratake, S., Yoshino, D., Kamm, R. D., & Funamoto, K. (2020). Microfluidic platform for three-dimensional cell culture under spatiotemporal heterogeneity of oxygen tension. *APL Bioengineering*, *4*(1), 016106. https://doi.org/10.1063/1.5127069

Kolmogorov, A., Petrovskii, I., & Piskunov, N. (1937). Etude de l'équation de la diffusion avec croissance de la quantité de matière et son application à un problème biologique. *Bull. Univ. Moskow, Ser. Internat., Sec. A*, *1*, 1–25. Retrieved from https://ci.nii.ac.jp/naid/10003528013

Lewis, D. M., Park, K. M., Tang, V., Xu, Y., Pak, K., Eisinger-Mathason, T. S. K., … Gerecht, S. (2016). Intratumoral oxygen gradients mediate sarcoma cell invasion. *Proceedings of the National Academy of Sciences of the United States of America*, *113*(33), 9292–9297. https://doi.org/10.1073/pnas.1605317113

Lyons, T. W., Reinhard, C. T., & Planavsky, N. J. (2014). The rise of oxygen in Earth's early ocean and atmosphere. *Nature*. Nature. https://doi.org/10.1038/nature13068

Muinonen-Martin, A. J., Susanto, O., Zhang, Q., Smethurst, E., Faller, W. J., Veltman, D. M., … Insall, R. H. (2014). Melanoma Cells Break Down LPA to Establish Local Gradients That Drive Chemotactic Dispersal. *PLoS Biology*, *12*(10). https://doi.org/10.1371/journal.pbio.1001966

Nakajima, A., Ishihara, S., Imoto, D., & Sawai, S. (2014). Rectified directional sensing in long-range cell migration. *Nature Communications*, *5*(1), 1–14. https://doi.org/10.1038/ncomms6367

Palecek, S. P., Loftust, J. C., Ginsberg, M. H., Lauffenburger, D. A., & Horwitz, A. F. (1997). Integrin-ligand binding properties govern cell migration speed through cell-substratum adhesiveness. *Nature*, *385*(6616), 537–540. https://doi.org/10.1038/385537a0

Pan, M., Xu, X., Chen, Y., & Jin, T. (2016). Identification of a Chemoattractant G-Protein-Coupled Receptor for Folic Acid that Controls Both Chemotaxis and Phagocytosis. *Dev Cell.*, *36*(4), 428–439. https://doi.org/10.1016/j.devcel.2016.01.012

Pugh, C. W., & Ratcliffe, P. J. (2017). New horizons in hypoxia signaling pathways. *Exp Cell Res*, *356*, 116–121.

Roques, L., Garnier, J., Hamel, F., & Klein, E. K. (2012). Allee effect promotes diversity in traveling waves of colonization. *Proceedings of the National Academy of Sciences of the United States of America*, *109*(23), 8828–8833. https://doi.org/10.1073/pnas.1201695109

Sandonà, D., Gastaldello, S., Rizzuto, R., & Bisson, R. (1995). Expression of Cytochrome c Oxidase during Growth and Development of Dictyostelium. *The Journal of Biological Chemistry*, *270*(10), 5587–5593.

Saragosti, J., Calvez, V., Bournaveas, N., Perthame, B., Buguin, A., & Silberzan, P. (2011). Directional persistence of chemotactic bacteria in a traveling concentration wave. *Proceedings of the National Academy of Sciences*, *108*(39), 16235–16240. https://doi.org/10.1073/pnas.1101996108

Stuelten, C. H. (2017). Moving in and Out: Dispersion of Cells in Self-Generated Gradients. *Journal of Clinical & Cellular Immunology*, *08*(03). https://doi.org/10.4172/2155-9899.1000507

Sussman, M. (1987). Cultivation and Synchronous Morphogenesis of Dictyostelium under Controlled Experimental Conditions. *Methods in Cell Biology*, *28*(C), 9–29. https://doi.org/10.1016/S0091-679X(08)61635-0

Swat, M. H., Thomas, G. L., Belmonte, J. M., Shirinifard, A., Hmeljak, D., & Glazier, J. A. (2012). Chapter 13 – Multi-Scale Modeling of Tissues Using CompuCell3D. In *Methods in Cell Biology* (Vol. 110, pp. 325–366). https://doi.org/10.1016/B978-0-12-388403-9.00013-8

Tonon, F., Giobbe, G. G., Zambon, A., Luni, C., Gagliano, O., Floreani, A., … Elvassore, N. (2019). In vitro metabolic zonation through oxygen gradient on a chip. *Scientific Reports*, *9*(September 2018), 13557. https://doi.org/10.1038/s41598-019-49412-6

Torija, P., Vicente, J. J., Rodrigues, T. B., Robles, A., Cerdán, S., Sastre, L., … Escalante, R. (2006). Functional genomics in Dictyostelium: MidA, a new conserved protein, is required for mitochondrial function and development. *Journal of Cell Science*, *119*(6), 1154–1164. https://doi.org/10.1242/jcs.02819

Tweedy, L., & Insall, R. H. (2020). Self-Generated Gradients Yield Exceptionally Robust Steering Cues. *Frontiers in Cell and Developmental Biology*, *8*. https://doi.org/10.3389/fcell.2020.00133

Tweedy, L., Susanto, O., & Insall, R. H. (2016, October 1). Self-generated chemotactic gradients - cells steering themselves. *Current Opinion in Cell Biology*. Elsevier Ltd. https://doi.org/10.1016/j.ceb.2016.04.003

Ungerböck, B., Charwat, V., Ertl, P., & Mayr, T. (2013). Microfluidic oxygen imaging using integrated optical sensor layers and a color camera. *Lab on a Chip*, *13*(8), 1593–1601. https://doi.org/10.1039/c3lc41315b

Van Haastert, P. J. M., Keizer-Gunnink, I., & Kortholt, A. (2017). Coupled excitable Ras and F-actin activation mediates spontaneous pseudopod formation and directed cell movement. *Molecular Biology of the Cell*, *28*(7), 922–934. https://doi.org/10.1091/mbc.E16-10-0733

Venkiteswaran, G., Lewellis, S. W., Wang, J., Reynolds, E., Nicholson, C., & Knaut, H. (2013). Generation and dynamics of an endogenous, self-generated signaling gradient across a migrating tissue. *Cell*, *155*(3), 674. https://doi.org/10.1016/j.cell.2013.09.046

Winn, K. M., Bourne, D. G., & Mitchell, J. G. (2013). Vibrio coralliilyticus Search Patterns across an Oxygen Gradient. *PLOS ONE*, *8*(7), 1–8. https://doi.org/10.1371/journal.pone.0067975

Xu, Y., Wang, Z. A., Green, R. S., & West, C. M. (2012). Role of the Skp1 prolyl-hydroxylation/glycosylation pathway in oxygen dependent submerged development of Dictyostelium. *BMC Developmental Biology*, *12*. https://doi.org/10.1186/1471-213X-12-31